International Journal of General Medicine

Dovepress
Taylor & Francis Group

Open Access Full Text Article

ORIGINAL RESEARCH

Identification of Ferroptosis-Related Genes in Patients with Renal Ischemia-Reperfusion Injury

Guangwei Jiang[1], Jikuan Li[1], Ruoyu Dong[1], Yuyan Chen[2], Xiaoyu Zhang[1], Xiaoming Shi[1]

[1]Department of Vascular Surgery, Hebei General Hospital, Shijiazhuang, Hebei Province, 050000, People's Republic of China; [2]Second Department of Rehabilitation Medicine, The Second Hospital of Hebei Medical University, Shijiazhuang, Hebei Province, 050051, People's Republic of China

Correspondence: Xiaoming Shi, Email shixm2021@outlook.com

Background: During acute kidney injury, hypoxic injury following reactive oxygen species (ROS) production due to reoxidation leads to severe inflammation and ferroptosis. Thus, the aim of the current research was to determine the ferroptosis-related biomarkers in IRI injury.

Methods: GSE43974 dataset was analyzed to identify differentially expressed genes (DEGs) using bioinformatics analysis. The intersection of DEGs and ferroptosis-related genes was identified as differentially expressed ferroptosis-related genes (DEFRGs). Finally, a renal ischemia-reperfusion model was made using mice, and the model was identified by HE staining and markers of IRI, including BUN and Scr. Changes in the expression of hub gene in the model and sham groups were detected by RT-pcr.

Results: A total of 3950 DEGs were identified between the IRI and control samples. Thereafter, 74 DEFRGs are obtained by taking the intersection of DEGs and ferroptosis-related genes. The GO analysis indicated that DEFRGs were mainly enriched in response to oxidative stress-related pathway. By MCODE, ATF3, ATF4, ATG3, ATG5, BECN1, DDIT3, HSPA5, NFE2L2, WIPI1, XBP1 were identified as hub genes. ATF3, DDIT3, ATF4, and ATG3 with AUC more than 0.7 were identified as biomarkers. It was confirmed by RT-pcr that the expression of hub genes ATF3, DDIT3, ATF4 was significantly elevated, and the expression of ATG3 was significantly reduced in the IRI model group. It was consistent with the expected results of data analysis in GEO.

Conclusion: In conclusion, our study identified 4 ferroptosis-related hub genes in the IRI and demonstrated that they are potential diagnostic biomarkers for IRI.

Keywords: acute kidney injury, IRI, hub gene, ferroptosis-related genes, ROS

Introduction

Acute Kidney Injury (AKI) is a clinical syndrome characterized by a rapid decline in renal excretory function over a period of hours to days, accompanied by an accumulation of nitrogenous metabolites (eg, creatinine and urea nitrogen) as well as other clinically unmeasurable wastes, with the primary clinical and laboratory manifestations being decreased urine output (which can also be polyuric),[1–3] accumulation of metabolic acids, and increased potassium and phosphate concentrations.[2] There is growing evidence that AKI is a risk factor for the development and/or accelerated progression of chronic kidney disease to end-stage renal disease.[4,5] However, current measures to prevent the development and/or progression of AKI are limited, and the search for specific drugs is hampered by late diagnosis and complex and incompletely elucidated pathophysiologic mechanisms.[2,6] Therefore, it is important to study the pathophysiologic mechanisms underlying the development and progression of AKI and to search for key aspects of AKI prevention and treatment. AKI is caused by a variety of etiologies, including sepsis, nephrotoxic drugs, rhabdomyolysis, and renal ischemia reperfusion (IRI) injury, among which IRI injury is one of the most common etiologies.[7,8]

It is currently believed that IRI injury is related to oxidative stress, mitochondrial dysfunction, intracellular calcium overload, and inflammation after ischemia-reperfusion.[9] Renal tubular epithelial cells are the main functional cells of the kidney and are susceptible to various factors such as hypoxia and toxins, etc. IRI injury leads to the production of large amounts of reactive oxygen species (ROS) by renal tubular epithelial cells, which triggers lipid peroxidation of the cell

Received: 3 March 2025
Accepted: 9 July 2025
Published: 17 July 2025

membrane as well as mitochondrial damage, resulting in cell death.[10] Recent studies have shown that renal tubular epithelial cells in AKI exhibit various forms of regulated necrosis: necrotic apoptosis, pyroptosis, ferroptosis, etc.[11] Among them, ferroptosis is the most studied form of regulated necrosis occurring in renal tubular epithelial cells in recent years.[12]

Ferroptosis, a mode of programmed cell death proposed by Stockwell in 2012, is mainly characterized by iron-dependent lipid peroxidation of the cell membrane.[13] Existing studies have shown that ferroptosis is involved in the development of a variety of diseases, such as neurodegenerative diseases, cancers immune diseases and ischemia-reperfusion injury.[13] One study found in the mouse that IRI induced ferroptosis by down-regulation of HMOX1 caused ferroptosis in renal tubular epithelial cells, leading to the development of AKI.[14] Therefore, effective inhibition of ferroptosis in renal tubular epithelial cells is expected to be a new idea for the prevention and treatment of AKI. Our study hopes to find reliable biomarkers for IRI by studying ferroptosis -related genes. It provides a valuable reference for the clinical diagnosis of IRI.

Materials and Methods

Data Source

The GSE43974 dataset was retrieved from the Gene Expression Omnibus (GEO) database. This dataset, based on the GPL10558 Illumina HumanHT-12 V4.0 expression beadchip, includes 105 ischemia-reperfusion injury (IRI) kidney tissue samples from brain-dead donors (T3 group) and 101 control kidney tissue samples (T1 group), as detailed in Supplementary Table 1. Additionally, 259 ferroptosis-related genes were sourced from the FerrDB database.

Screening of DEGs

The R package limma was used for DEG analysis. We perceived adj.P < 0.05 to be statistically significant for the DEGs, and logFC≥1 and logFC≤1 were used to indicate upregulated and downregulated DEGs. We constructed volcano plots and heatmaps using the R packages ggplot2 and pheatmap, respectively. The intersections between DEGs and ferroptosis-related genes were identified using the "VennDiagram" R package and were defined as DEFRGs for subsequent analysis.

Functional Enrichment Analysis

KEGG is a database resource for elucidating high-level functions and effects of biological systems. GO a powerful tool to analyze the cellular component (CC), biological function (BP) and molecular function (MF) of DEFRGs. GO and KEGG pathway enrichment analysis using the clusterProfiler package were used to explore the function of DEFRGs.

PPI Network Construction

The differentially expressed ferroptosis-related genes (DEFRGs) were uploaded to the STRING database (http://www.string-db.org/) to construct a protein–protein interaction (PPI) network. Subsequently, we used Cytoscape software to screen hub genes through MCODE plug-in. Expression levels of hub genes between IRI and control samples in GSE43974 were shown using boxplots.

Receiver Operating Characteristic (ROC) Curve Analysis

We used the "pROC" R package to construct ROC curves. ROC analyses were estimated the role of hub genes in the diagnosis of IRI. When the area under the curve (AUC) value was >0.7, the hub genes were considered to be capable of distinguishing IRI from control with excellent specificity and sensitivity. Hub genes with an AUC value of > 0.7 were used as biomarkers. The semantic similarities of gene classes were calculated using the "GOSemSim" package. Corrplot package was used to analyze the correlation of biomarkers.

Construction of Genes-miRNA/TF Regulatory Network

In this study, we selected miRNet database to predict the regulatory relationship between genes and miRNAs/TFs. Subsequently, the TF/miRNA-target gene regulatory network was visualized by Cytoscape software. In the network, a blue node represents the genes, a purple node represents the TF, and an orange node represents the miRNA.

Experiments on Animals

Six SD rats (male, SPF class), weight range 250–300 g, age 8–10w. The six SD rats (male) were grouped according to the randomized numerical method (three rats in each group): sham operation group (Sham group) and IRI group. All experimental animals were housed in a standardized environment and were not allowed to drink or eat for 12 h. The renal IRI model was replicated by non-invasive arterial clamping of both renal pedicles. The rats in each group were anesthetized by intraperitoneal injection of 10% chloral hydrate (5mg/kg). No rats exhibited signs of peritonitis after the intraperitoneal administration of 10% chloral hydrate, and an incision of about 2cm as made in the middle of the abdomen of the rats with surgical scissors. After the bilateral renal pedicles were exposed, non-invasive arterial clamps were used to block the blood supply for 0.5 h. After 45 min, the vascular clip was released, and the color of both kidneys returned to red, indicating that renal blood flow was restored to perfusion, and the renal ischemia-reperfusion model was successfully modeled. The incision was sutured and reperfused for 24 h. The arterial clamps were loosened to restore the blood flow supply, complete the reperfusion of the blood flow, and suture the incisions; no arterial clamps were used in the sham operation group. Close operation, other operations are the same. The experiment was approved by the Ethics Committee of Hebei Provincial People's Hospital (Approval Number: 2023100), and it was conducted in accordance with the Animal Welfare Ethics of Hebei Provincial People's Hospital.

Specimen Collection

Rats in each group were fully anesthetized with intraperitoneal injection of 3 mg/mL sodium pentobarbital (50 mg/kg) 12 to 24 hours after surgery and then fixed on their backs on the operating table. After routine disinfection, femoral venous blood was centrifuged and the supernatant was taken. Urea nitrogen (BUN), blood creatinine (Scr) was tested with a fully automatic biochemical instrument. The rats were then sacrificed, and the kidneys were removed and quickly stored at −80°C for subsequent experiments. After kidney tissue removal, the experimental animals were euthanized according to the 3R principle. The specific procedure is as follows: cervical dislocation is performed in the animal under deep anesthesia. Confirm that the animal stops breathing, nerve reflexes disappear, and muscles relax.

Tissue HE Staining

The left kidneys of the mice in the model group and the sham operation group were harvested, fixed with 4% paraformaldehyde, dehydrated with graded ethanol, and made transparent with xylene. Organ tissue sections were stained. Observe and take photos with an optical microscope.

BUN and Scr Level Detection

Twenty-four hours after surgery, blood was collected from the abdominal aorta, serum was separated by centrifugation, and stored in a −80°C refrigerator for later use. The urease glutamate dehydrogenase method and sarcosine oxidase method were used to detect rat serum BUN and Ser levels, respectively. Blood Urea Nitrogen (BUN) and creatinine levels were measured in serum/plasma samples using standardized automated assays. BUN was quantified via the urease/GLDH enzymatic method (Roche Diagnostics, Germany), wherein urea hydrolysis by urease releases ammonia, which is subsequently coupled to α-ketoglutarate by glutamate dehydrogenase (GLDH), with NADH oxidation monitored spectrophotometrically at 340 nm. Creatinine was assessed using the modified Jaffé kinetic method (Siemens Advia 1800 analyzer), which mitigates interference from non-creatinine chromogens by measuring absorbance changes at 505 nm at two timepoints (20 and 80 seconds). Calibration curves were generated using IDMS-traceable standards, and daily quality controls (Bio-Rad) confirmed intra-assay CVs <3%. Hemolyzed or lipemic samples were excluded to ensure accuracy.

RT-PCR Detection of Hub Gene Expression in Kidney Tissue

The total RNA extraction, reverse transcription, and RT-qPCR steps refer to the TRIzol kit, TaKaRa kit, and TB Green PremixEx Tag™ II kit, respectively. SYBR Green qPCR system (10 μL): 0.5 μL each of forward and reverse primers, 5 uL of SYBR premix Ex Tag"(2x), 2 μL of RNase Freed H,0, and 2 μL of sample cDNA. The reaction conditions were set as follows: 95 °C 1.5 min; 95 °C 5s, 60 °C 30s, 40 cycles; 65 °C 2s. The primer sequences were designed as follows, and all primers were synthesized by Sangon Biotech (Shanghai, China). ATF: F-CAGCCAGCAACCTCAGACTC, R-TGGGTGGTGGTAGTCAGTCC; DDIT3: F-AGCCAAAATCAGAGCTGGAAAC, R-TGGATCAGTCTGGAAAAGCA; ATF4: F-GCCCTTTACCAACAGCAAGG, R-GCTGGAAAACCAATCTGTCC; ATG3: F-TGCCTTCGACCTCTACATCG, R-CAGGTCCAGGTAGCCATTGT.

Statistical Analysis

All statistical analyses were performed using GraphPad Prism 9.0 (GraphPad Software, USA) and R 4.2.0. For comparison between two experimental groups, Student's *t*-test (for normally distributed data) or Mann–Whitney *U*-test (for non-parametric data) was applied. Multiple group comparisons were conducted using one-way ANOVA followed by Tukey's post hoc test.

Results

Identification of DEGs

GSE43974 was downloaded from GEO, and we compared IRI patients with controls to obtain DEGs. A total of 3950 DEGs were screened, which consisted of 1102 up-regulated genes and 2848 down-regulated genes (IRI vs Control) (Figure 1A). The heatmap for DEGs was shown in Figure 1B. In both the IRI group and the Control group, Ferroptosis scores were calculated using the Ferroptosis Driver genes from the FerrDB database and assessed via the ssGSEA method. The boxplot illustrating intergroup differences is shown in Figure 1C. Notably, the Ferroptosis pathway scores in the IRI group were significantly higher than those in the Control group, further indicating the role of Ferroptosis in IRI.

Identification and Functional Enrichment Analysis of DEFRGs

Seventy-four DEFRGs were obtained by taking the intersection of DEGs and ferroptosis-related genes. The Venn diagram of DEFRGs was shown in Figure 2A. GO analysis (Figure 2B) indicated that DEFRGs were mainly enriched in response to oxidative stress, cellular response to chemical stress, response to nutrient levels, cellular response to oxidative stress. The KEGG enrichment analysis (Figure 2C) showed that these DEFRGs were significantly involved in mitophagy-animal, kaposi sarcoma-associated herpesvirus infection, autophagy-animal, IL−17 signaling pathway.

PPI Network and Hub Genes Identification

The PPI network of DEFRGs was established using the STRING database (Figure 3A). Ten hub genes (ATF3, ATF4, ATG3, ATG5, BECN1, DDIT3, HSPA5, NFE2L2, WIPI1, XBP1) were identified by MCODE plug-in (Figure 3B). We explored the expressions of hub genes between IRI and control samples and found that ATF3, ATF4, DDIT3, HSPA5, NFE2L2, and XBP1 exhibited higher expression levels in IRI, while ATG3, ATG5, BECN1, and WIPI1 exhibited lower expression levels in IRI (Figure 4). As shown in Figure 5, the AUC values of ATF3, DDIT3, ATF4, and ATG3 were 0.997, 0.958, 0.798, and 0.708, respectively, demonstrating that these hub genes had good diagnostic values. Furthermore, we conducted a comprehensive analysis of network topological properties for each protein-protein interaction, including Average Shortest Path Length, Betweenness Centrality, Closeness Centrality, Clustering Coefficient, Degree, Eccentricity, Neighborhood Connectivity, and Number of Undirected Edges. The complete dataset of these network parameters has been systematically compiled and presented in Supplementary Table 2.

The Functional Similarity Analysis

In order to achieve a better understanding of the molecular mechanism of the 4 biomarkers, we performed a functional similarity analysis of these genes. As shown in Figure 6A, DDIT3 and ATF4 were identified as the top two genes with the

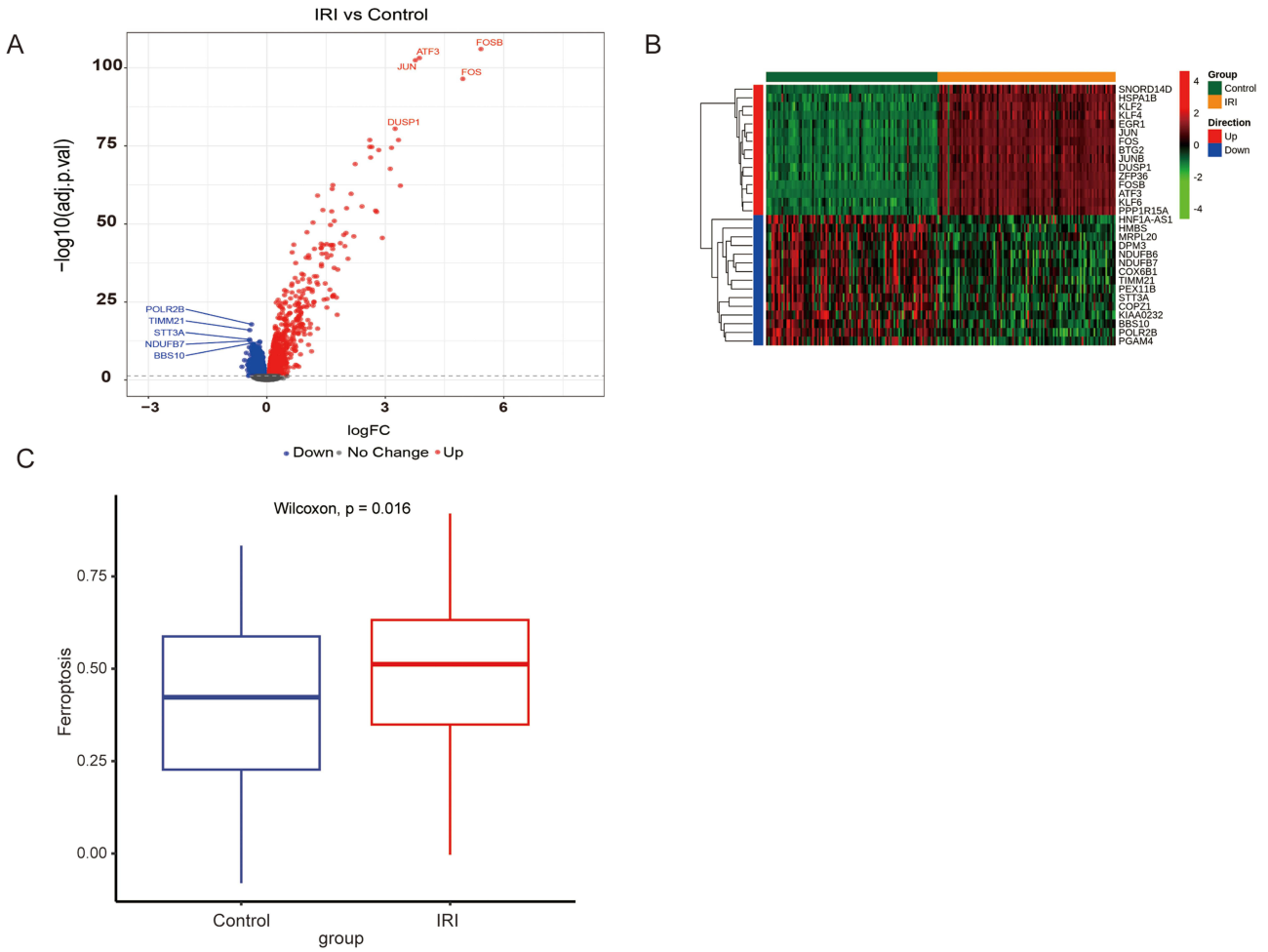

Figure 1 The differential expression genes identified by limma R package between IRI patients and normal control. (**A**) Volcano plot for the differential expression analysis, blue for down-regulate gene, red for up-regulate. (**B**) Heatmap for the top 15 up-regulated genes and top 15 down-regulated genes as sorted by adjusted p-value.(**C**). Ferroptosis-related pathway score.

highest-ranking scores. Correlation analysis of these genes was performed using the GSE43974 dataset. Among them, DDIT3 and ATF3 exhibited the strongest correlation, with a value of 0.87 (Figure 6B).

Prediction of Potential miRNA/TF-Hub Gene Regulatory Network

As illustrated in Figure 7, the interaction network consists of 4 biomarkers, 124 miRNAs, and 30 TFs. Then, a miRNA/TF-gene regulatory network was constructed using Cytoscape to understand the possible transcriptional regulation mechanism of hub genes. The genes that were regulated by the largest number of miRNAs were ATF4, which was regulated by 49 miRNAs. And ATF3 were the hub genes regulated by the largest number of TFs, which was regulated by 19 TFs.

In vivo Experiments to Verify Hub Gene Expression

To verify that key genes are differentially expressed in IRI. We made IRI model mice. It was found that the expression of IRI serum marker genes BUN and Scr in the IRI group significantly higher than that in the sham surgery group (Figure 8A), HE staining showed that the renal tissue morphology of the rats in the sham operation group was normal, without degeneration and necrosis, the renal tubular epithelial cells were plump, and the renal tubular lumen was not dilated; the renal tissue of the rats in the IRI group showed severe damage and vacuolar degeneration of the renal tubular epithelial cells, swelling and shedding, renal tubule lumen expansion, obvious infiltration of inflammatory cells, renal

https://doi.org/10.2147/IJGM.S522363

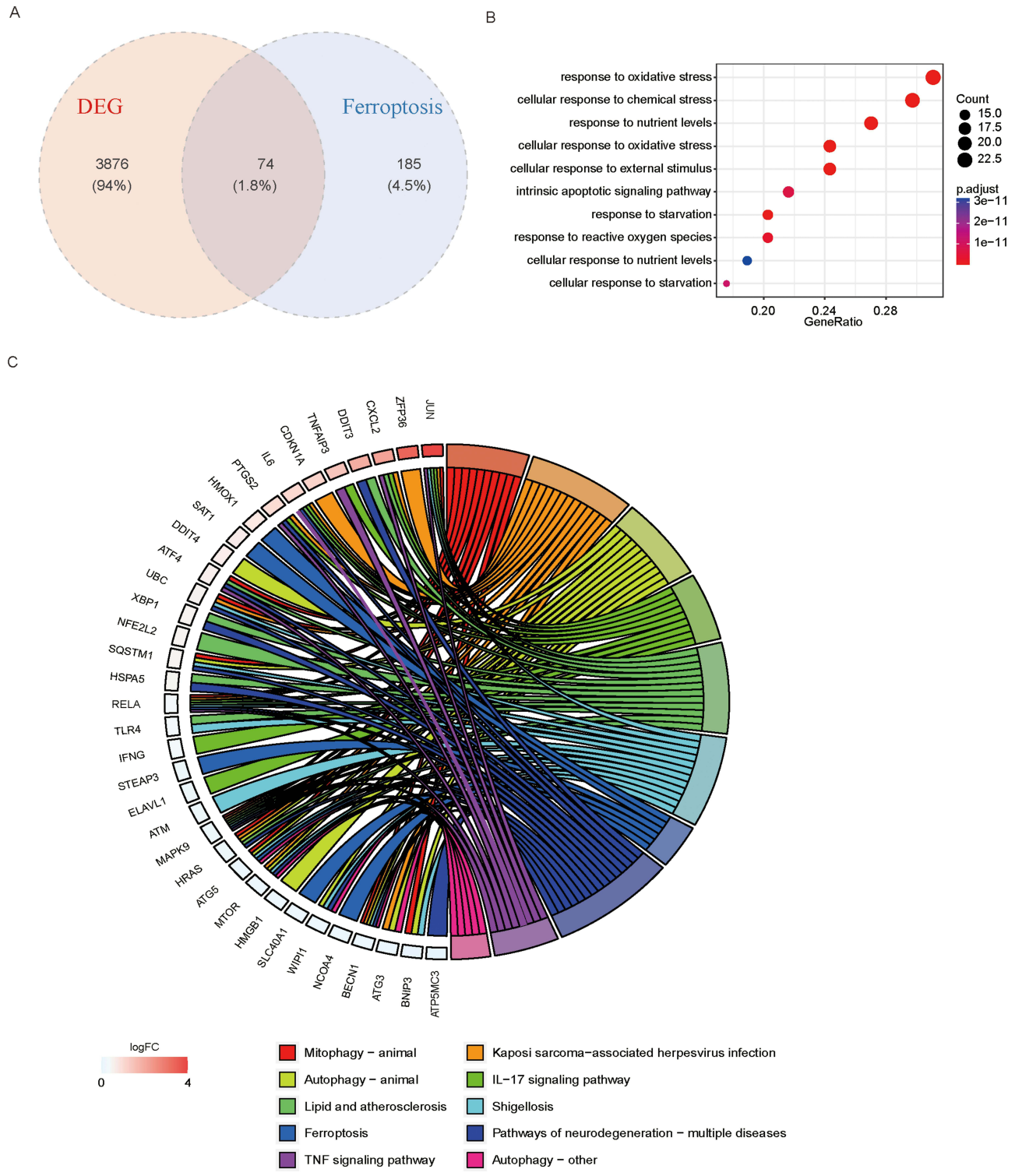

Figure 2 Differential genes associated with immunity. (**A**) The Venn diagram shows the intersection of DEG and ferroptosis-related genes. (**B**) GO enrichment results (**C**) KEGG enrichment results.

interstitial congestion and edema (Figure 8B). The histological assessment was performed qualitatively by evaluating morphological features (eg, tubular necrosis, inflammatory infiltration) rather than using quantitative scoring systems, as our study focused on characterizing the injury patterns rather than measuring their extent numerically. It indicated that the IRI model was successful.

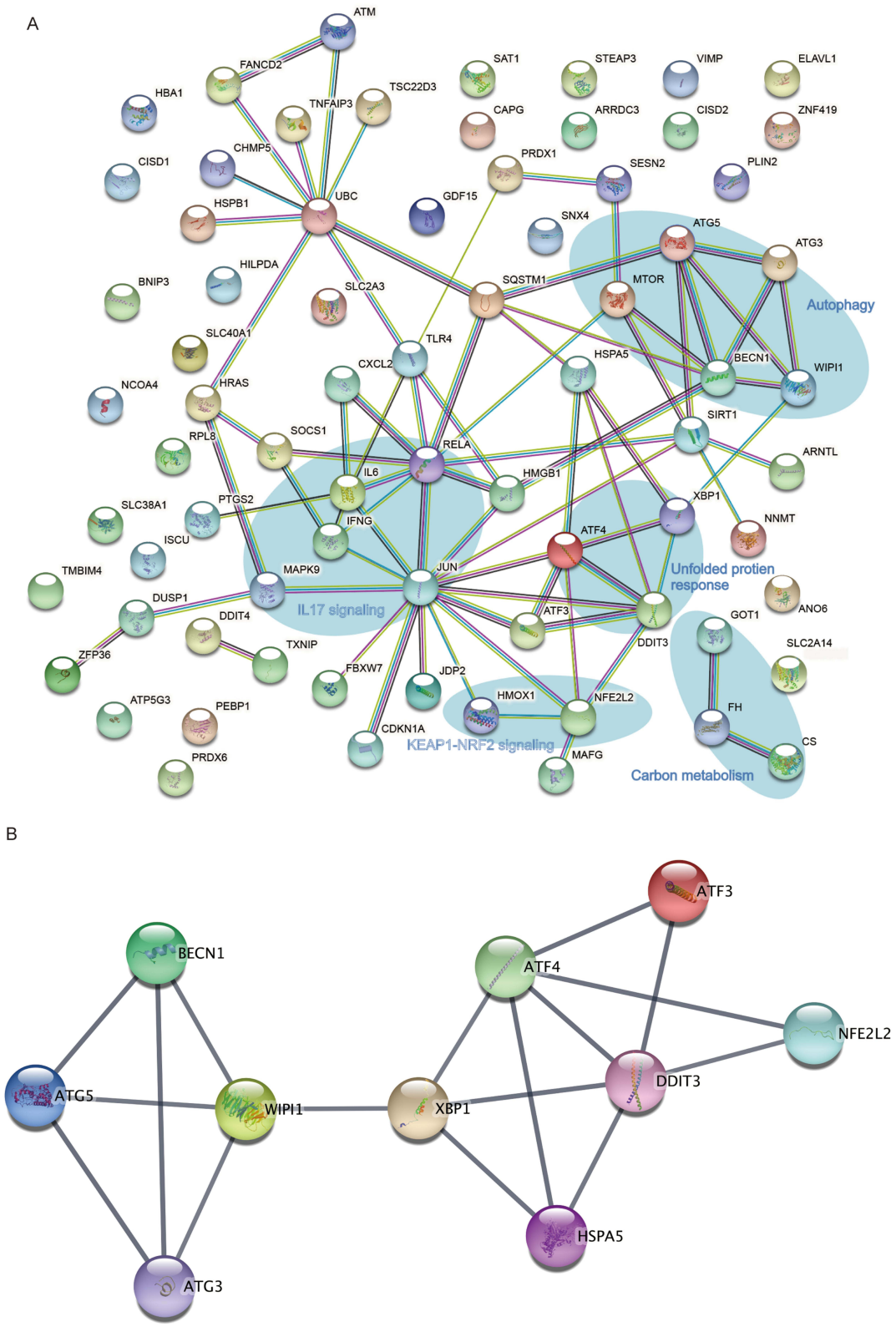

Figure 3 Protein network interaction and screening of key modules. (**A**) PPI protein network interaction diagram. (**B**) PPI network diagram of 10 hub genes from core module analyzed using MCODE.

https://doi.org/10.2147/IJGM.S522363

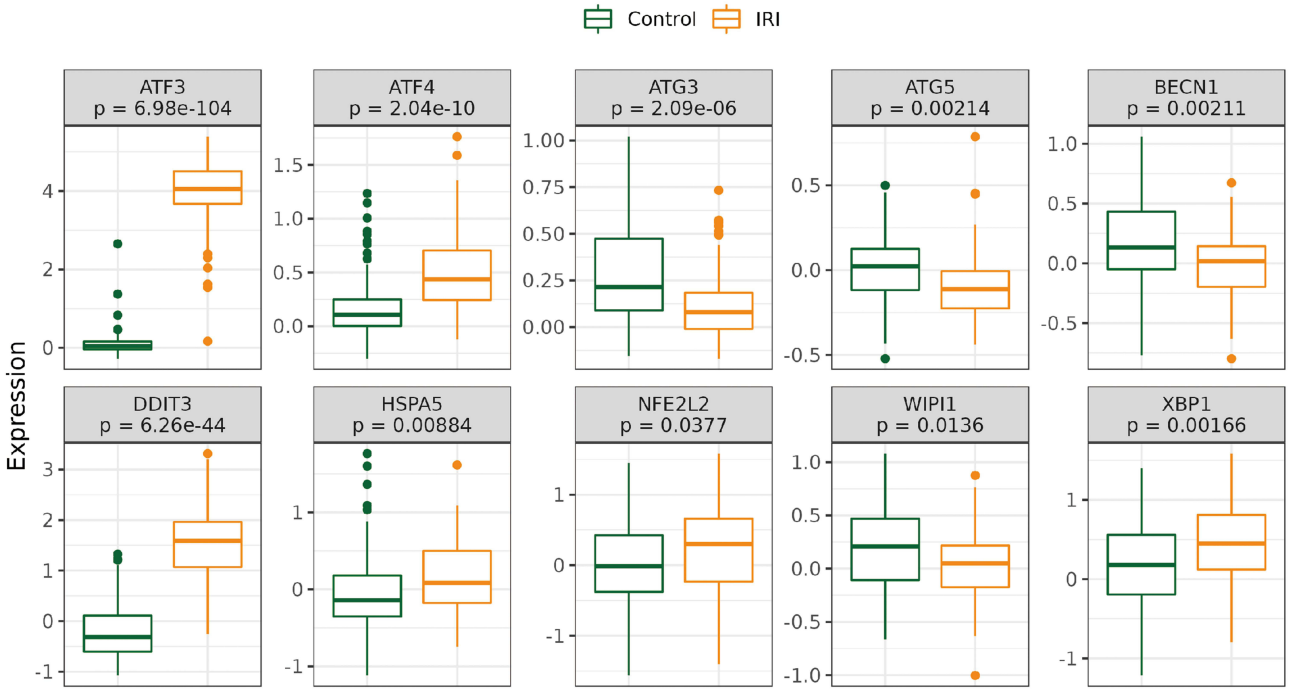

Figure 4 Evaluation of the diagnostic effect of hub gene on IRI. Ten genes were expressed in both groups.

We further explored the difference in the expression of hub genes between the model group and the sham-operated group, and found that the expression of three hub genes, ATF3, DDIT3 and ATF4, was significantly higher in the IRI group than in the Sham group, while the expression of ATG3 was significantly lower in the IRI group than in the sham group, which was in agreement with our predicted results (Figure 8C). This indicates that these four hub genes play important roles in the development of IRI and have the potential to become IRI biomarkers.

Discussion

The kidney is highly sensitive to inadequate perfusion, and shock, trauma, transplantation and other factors often cause IRI injury in critically patients, leading to AKI.[15] The current popular gene sequencing technology reveals genetic changes in genes during the progression of various diseases, which provides the possibility of exploring the gene expression abnormalities in early IRI injury and finding effective methods to treat early AKI. In this study, we downloaded the IRI dataset GSE43974 from the GEO database, and used bioinformatics methods to screen the DEGs of IRI and control. These results provide an important foundation for the future search of biomarkers for IRI.

Iron death-related genes that play a key role in IRI were identified in this study by multiple bioinformatics approaches, including PPI networks. And ATF3, ATF4, ATG3, ATG5, BECN1, DDIT3, HSPA5, NFE2L2, WIPI1, XBP1 were found to be hub genes. Based on the results of ROC, ATF3, DDIT3, ATF4, ATG3 showed high sensitivity and specificity for IRI, suggesting that they can be used as biomarkers for the diagnosis of IRI. The role of some of these genes in IRI has been reported. ATF3 has been demonstrated to play a dual role in renal I/R injury, where it can either promote tubular cell apoptosis through ER stress activation or exert protective effects against oxidative damage depending on cellular context.[16,17] Pan's study found that Atf3 could be a potential drug target in IRI.[18] ATF4, another key ER stress transducer, has been shown to exacerbate renal tubular injury by promoting oxidative stress and inflammatory responses.[19] VDR attenuated I/R-induced AKI by suppressing ERS partly via transcriptional regulation of ATF4. VDR attenuated I/R-induced AKI by suppressing ERS partly via transcriptional regulation of ATF4.[20] Sheng's study likewise predicted DDIT3 as the hub gene for the IRI process via the GEO database.[21] Similarly, DDIT3 (CHOP) is a well-established mediator of ER stress-induced apoptosis in renal tubules, with DDIT3-deficient mice showing significant protection against I/R injury.[22] Recent studies have further connected DDIT3 to ferroptosis regulation in

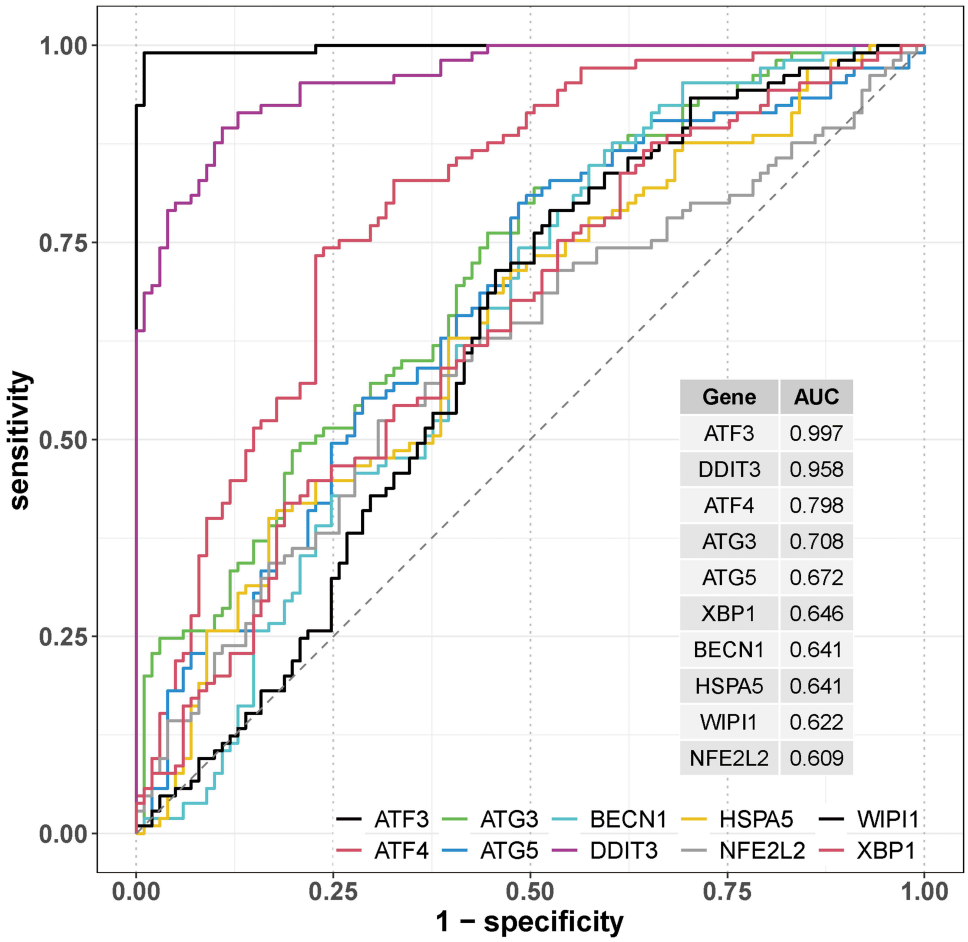

Figure 5 ROC curves and AUC values of the 10 hub genes.

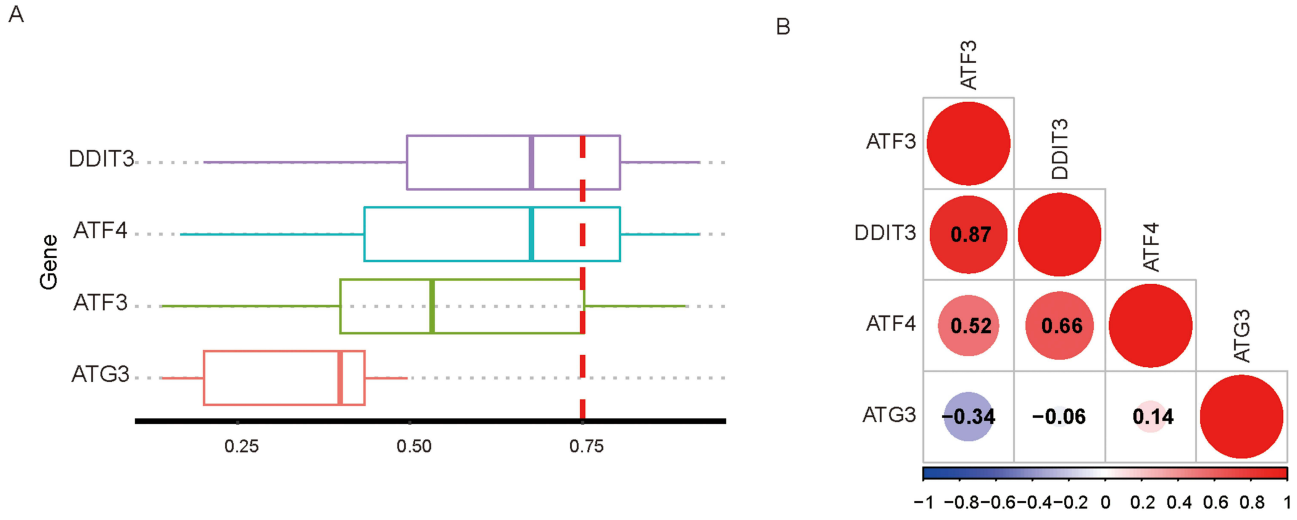

Figure 6 The functional similarity analysis. (**A**) Hub gene semantic similarity analysis (**B**) The correlations among hub genes.

renal I/R through modulation of lipid peroxidation pathways.[23] ATG3, although not proven to play a role in IRI, has been shown in numerous studies to regulate processes such as nephropathy by modulating the autophagic process.[24–26] Interestingly, ATG3's role in renal I/R appears more complex, with evidence suggesting it may participate in both protective autophagy and autophagic cell death pathways.[27] All of the above results corroborate the possibility of these

https://doi.org/10.2147/IJGM.S522363

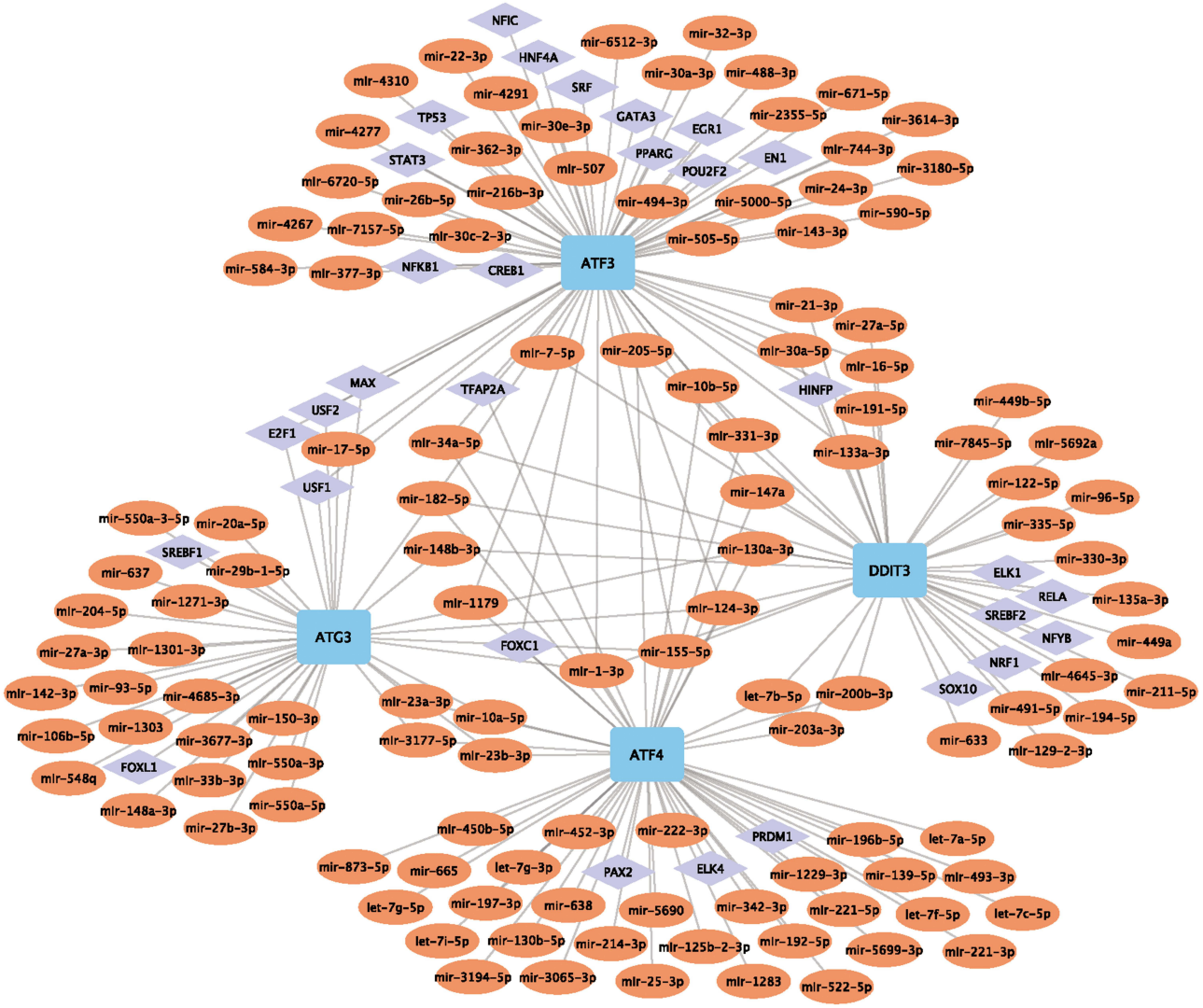

Figure 7 Construction of miRNA-gene-TF regulatory network. Light blue rectangle for hub genes, Orange oval for miRNA, purple diamond for TF.

several hub genes as biomarkers for IRI. Our study not only validated these hub genes using external datasets but also validated the in vivo expression of these hub genes for the first time, increasing the credibility of the results. These literature findings not only validate our bioinformatics predictions but also provide mechanistic insights into how these hub genes may contribute to renal I/R injury through multiple interconnected pathways, including ER stress, oxidative damage, and programmed cell death processes. The consistent association of these genes with renal I/R injury across independent studies strengthens the biological relevance of our findings and highlights their potential as therapeutic targets. Future studies should focus on elucidating the precise molecular mechanisms and potential crosstalk between these regulatory genes in different phases of renal I/R injury.

However, our study found potential biomarkers for IRI (ATF3, DDIT3, ATF4, and ATG3) and validated their expression. This is important for the early diagnosis of IRI. However, if we consider their future application as therapeutic targets in the clinical treatment of IRI, we need to have a detailed delineation of the mechanism of action of these hub genes, which is partly the shortcoming of this study. We will further investigate the mechanism of action of these hub genes in future studies using existing animal models of IRI.

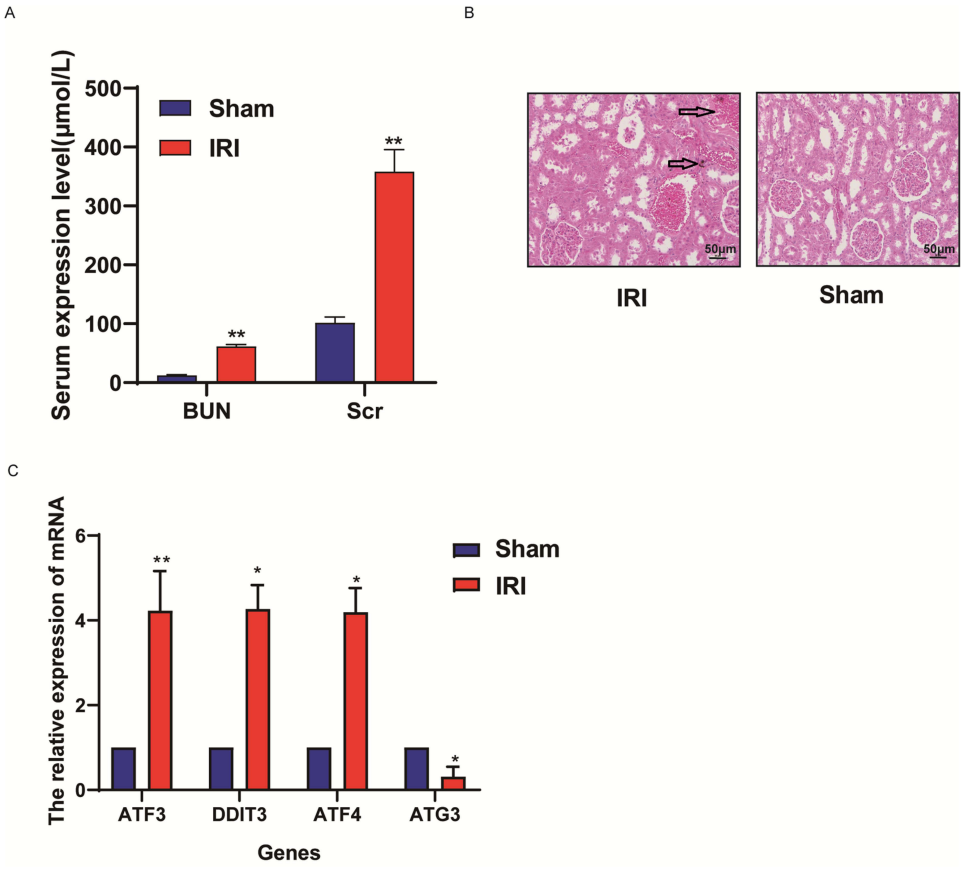

Figure 8 RT-qPCR validation of hub gene expression: (**A**) Serum expression of BUN and Scr levels. (**B**) HE staining of kidney tissue in IRI group and Sham group, The arrow indicates inflammatory infiltration. (**C**) mRNA expression of hub gene was evaluated in tissue by qRT-PCR (*$P < 0.05$, **$P < 0.01$).

Conclusion

Based on our study, we identified four ferroptosis-related hub genes in ischemia-reperfusion injury (IRI) and demonstrated their potential as diagnostic biomarkers for IRI. Additionally, these findings provide new insights into the molecular mechanisms underlying ferroptosis in the context of IRI, suggesting that these genes could also serve as therapeutic targets for the development of novel interventions. Future research focusing on the validation of these biomarkers and exploring their roles in ferroptosis regulation may further enhance our understanding of IRI pathogenesis and improve clinical outcomes.

Data Sharing Statement

The datasets for this study can be found in the GEO database. GSE43974, the original sequenced samples in GEO are tissue type samples. This paper has been uploaded to Research square as a preprint https://www.researchsquare.com/article/rs-2601585/v1.

Consent for Publication

GEO belongs to public databases. The patients involved in the database have obtained ethical approval. Users can download relevant data for free for research and publish relevant articles. Our study is based on open source data, so there are no ethical issues and other conflicts of interest. The experimental protocol was established, according to the ethical guidelines of the Helsinki Declaration and was approved by the Human Ethics Committee of Hebei General Hospital.

Acknowledgments

We sincerely acknowledge the contributions from the GEO datasets.

Author Contributions

All authors made a significant contribution to the work reported, whether that is in the conception, study design, execution, acquisition of data, analysis and interpretation, or in all these areas; took part in drafting, revising or critically reviewing the article; gave final approval of the version to be published; have agreed on the journal to which the article has been submitted; and agree to be accountable for all aspects of the work.

Funding

There is no funding to report.

Disclosure

The authors declare no potential conflicts of interest in this work.

References

1. Adebayo D, Wong F. Pathophysiology of hepatorenal syndrome - acute kidney injury. *Clin Gastroenterol Hepatol*. 2023;21(10S):S1–S10. doi:10.1016/j.cgh.2023.04.034
2. Duong N, Kakadiya P, Bajaj JS. Current pharmacologic therapies for hepatorenal syndrome-acute kidney injury. *Clin Gastroenterol Hepatol*. 2023;21(10S):S27–S34. doi:10.1016/j.cgh.2023.06.006
3. Zamirpour S, Hubbard AE, Feng J, Butte AJ, Pirracchio R, Bishara A. Development of a machine learning model of postoperative acute kidney injury using non-invasive time-sensitive intraoperative predictors. *Bioengineering*. 2023;10(8):932. doi:10.3390/bioengineering10080932
4. Liu M, Zhang Y, Ye Z, et al. Inflammatory bowel disease with chronic kidney disease and acute kidney injury. *Am J Prev Med*. 2023;65(6):1103–1112. doi:10.1016/j.amepre.2023.08.008
5. Sun L, Hua RX, Wu Y, Zou LX. Acute kidney injury in hospitalized adults with chronic kidney disease: comparing the reference change value of the serum creatinine optimized criteria for acute kidney injury in chronic kidney disease (cROCK), Kidney Disease Improving Global Outcomes (KDIGO), and combined criteria. *Kidney Res Clin Pract*. 2023;42(5):639. doi:10.23876/j.krcp.22.161
6. Habshi T, Shelke V, Kale A, Lech M, Gaikwad AB. Hippo signaling in acute kidney injury to chronic kidney disease transition: current understandings and future targets. *Drug Discov Today*. 2023;28(8):103649. doi:10.1016/j.drudis.2023.103649
7. Karimi F, Maleki M, Nematbakhsh M. View of the renin-angiotensin system in acute kidney injury induced by renal ischemia-reperfusion injury. *J Renin Angiotensin Aldosterone Syst*. 2022;2022:9800838. doi:10.1155/2022/9800838
8. Mohamed ME, Tawfeek N, Elbaramawi SS, Elbatreek MH, Fikry E. Agathis robusta bark extract protects from renal ischemia-reperfusion injury: phytochemical, in silico and in vivo studies. *Pharmaceuticals*. 2022;15(10):1270. doi:10.3390/ph15101270
9. Du Y, Ning JZ. MiR-182 promotes ischemia/reperfusion-induced acute kidney injury in rat by targeting FoxO3. *Urol Int*. 2021;105(7–8):687–696. doi:10.1159/000515649
10. Vormann MK, Tool LM, Ohbuchi M, et al. Modelling and prevention of acute kidney injury through ischemia and reperfusion in a combined human renal proximal tubule/blood vessel-on-a-chip. *Kidney360*. 2022;3(2):217–231. doi:10.34067/KID.0003622021
11. Li Z, Xu K, Zhang N, et al. Overexpressed SIRT6 attenuates cisplatin-induced acute kidney injury by inhibiting ERK1/2 signaling. *Kidney Int*. 2018;93(4):881–892. doi:10.1016/j.kint.2017.10.021
12. Zhao Z, Wu J, Xu H, et al. XJB-5-131 inhibited ferroptosis in tubular epithelial cells after ischemia-reperfusion injury. *Cell Death Dis*. 2020;11(8):629. doi:10.1038/s41419-020-02871-6
13. Shah R, Margison K, Pratt DA. The potency of diarylamine radical-trapping antioxidants as inhibitors of ferroptosis underscores the role of autoxidation in the mechanism of cell death. *ACS Chem Biol*. 2017;12(10):2538–2545. doi:10.1021/acschembio.7b00730
14. Friedmann Angeli JP, Schneider M, Proneth B, et al. Inactivation of the ferroptosis regulator Gpx4 triggers acute renal failure in mice. *Nat Cell Biol*. 2014;16(12):1180–1191. doi:10.1038/ncb3064
15. Vats K, Kruglov O, Mizes A, et al. Keratinocyte death by ferroptosis initiates skin inflammation after UVB exposure. *Redox Biol*. 2021;47:102143. doi:10.1016/j.redox.2021.102143
16. Zhu B, Ni Y, Gong Y, et al. Formononetin ameliorates ferroptosis-associated fibrosis in renal tubular epithelial cells and in mice with chronic kidney disease by suppressing the Smad3/ATF3/SLC7A11 signaling. *Life Sci*. 2023;315:121331. doi:10.1016/j.lfs.2022.121331
17. Melo Ferreira R, Sabo AR, Winfree S, et al. Integration of spatial and single-cell transcriptomics localizes epithelial cell-immune cross-talk in kidney injury. *JCI Insight*. 2021;6(12). doi:10.1172/jci.insight.147703
18. Pan Z, Yang Y, Cao R, et al. Identification and verification of potential biomarkers in renal ischemia-reperfusion injury by integrated bioinformatic analysis. *Biomed Res Int*. 2023;2023:7629782. doi:10.1155/2023/7629782
19. Cheng R, Wang X, Huang L, et al. Novel insights into the protective effects of leonurine against acute kidney injury: inhibition of ER stress-associated ferroptosis via regulating ATF4/CHOP/ACSL4 pathway. *Chem Biol Interact*. 2024;395:111016. doi:10.1016/j.cbi.2024.111016
20. Tang S, Wu X, Dai Q, et al. Vitamin D receptor attenuate ischemia-reperfusion kidney injury via inhibiting ATF4. *Cell Death Discov*. 2023;9(1):158. doi:10.1038/s41420-023-01456-4
21. He S, He L, Yan F, et al. Identification of hub genes associated with acute kidney injury induced by renal ischemia-reperfusion injury in mice. *Front Physiol*. 2022;13:951855. doi:10.3389/fphys.2022.951855

22. Li S, Yang Y, Shi MH, Wang JF, Ran XQ. miR-96-5p attenuates malathion-induced apoptosis of human kidney cells by targeting the ER stress marker DDIT3. *J Environ Sci Health B*. 2020;55(12):1080–1086. doi:10.1080/03601234.2020.1816092
23. Cao Y, Hu L, Chen R, Chen Y, Liu H, Wei J. Unfolded protein response-activated NLRP3 inflammasome contributes to pyroptotic and apoptotic podocyte injury in diabetic kidney disease via the CHOP-TXNIP axis. *Cell Signal*. 2025;130:111702. doi:10.1016/j.cellsig.2025.111702
24. Nuta GC, Gilad Y, Goldberg N, et al. Identifying a selective inhibitor of autophagy that targets ATG12-ATG3 protein-protein interaction. *Autophagy*. 2023;19(8):2372–2385. doi:10.1080/15548627.2023.2178159
25. Tanida I, Sou YS, Minematsu-Ikeguchi N, Ueno T, Kominami E. Atg8L/Apg8L is the fourth mammalian modifier of mammalian Atg8 conjugation mediated by human Atg4B, Atg7 and Atg3. *FEBS J*. 2006;273(11):2553–2562. doi:10.1111/j.1742-4658.2006.05260.x
26. Wang B, Qian JY, Tang TT, et al. VDR/Atg3 axis regulates slit diaphragm to tight junction transition via p62-mediated autophagy pathway in diabetic nephropathy. *Diabetes*. 2021;70(11):2639–2651. doi:10.2337/db21-0205
27. Ye Y, Tyndall ER, Bui V, et al. Multifaceted membrane interactions of human Atg3 promote LC3-phosphatidylethanolamine conjugation during autophagy. *Nat Commun*. 2023;14(1):5503. doi:10.1038/s41467-023-41243-4